Electromagnetic and thermal characterization of a new alloy of ferromagnetic material of Cobalt Vanadium Iron

Joaquim da Luz Lopes Ferreira

Instituto Superior Técnico, Universidade de Lisboa, Portugal

***Abstract* — This work focuses on the electromagnetic and thermal characterization of a new alloy of Cobalt-Vanadium-Iron ferromagnetic material, called Hyperco50 (Hy50). In general, in the new alloy Hy50, which has high magnetic permeability and higher magnetic saturation point of the typical ferromagnetic materials used in electric machines. Experimental tests were performed to study their characteristics. These Hy50 alloys can be processed to improve their magnetic properties, allowing their use in high performance energy conversion applications. Analytical models were developed to simulate the behavior of Hy50 in the magnetic circuit of a transformer. The results showed that the Hy50 can increase the density of the device, but requires an additional cooling system due to its high losses of iron.**

Keywords: Performance; BH curve; Iron losses.

I. INTRODUCTION

The continued demand for cheaper and more efficient electric motors has been a current challenge for the scientific and industrial community. Due to the need to reach new objectives, it was decided to study new materials to achieve the current goals. With new magnetic composite materials and superconducting materials, the goal is to increase the current electromagnetic limits of electrical machines. The Hyperco50 alloy (a composite of Vanadium-Cobalt-Iron) has higher magnetic properties than other commercial ferro-cobalt magnetic alloys [1],
[2]. Due to its characteristics and its high point of magnetic saturation, in recent decades this alloy has been characterized and studied in detail [3]-[16]. The manufacture of rotor and stator laminations in motors and generators for aircraft power generation applications have been already considering the use of Hy50 alloy.
The use of superconductors allows higher levels of magnetization than conventional permanent magnets. The discovery of the potential of these superconducting materials, leads to the construction of several types of electrical machines called Superconducting Machines. These possibilities, as well as other hypotheses about the material of Hy50, are still under study due to the complexity of the theme and the implementation of this type of material. The objective of this work is to deepen and consolidate its theoretical and practical knowledge framework related to the new magnetic alloys and its performance in a single-phase power transformer.

II. STATE OF ART

In this chapter it is described the main applications with ferromagnetic materials in electrical machines, and their main limitations, derived from losses in conductive materials and in the magnetic core.

A. New Superconducting Materials and Magnetic Compounds

To overcome the aforementioned limits, they suggest studies on new high temperature critical superconducting materials (SATC) and magnetic composite materials such as Hy50. From a saturation point of view, the Hy50 shows a saturation point increase for the 2.4T and also low iron losses.

1) Superconductivity.

The High Temperature Superconductors (HTS) are materials that reach the superconductivity state above 70ºK, allowing the use of liquid nitrogen to cool them. The use of HTS in electric machines allows the replacement of classical excitation systems, as permanent magnets, reducing magnetic dispersion when used as a "magnetic screen", and substituting typically copper windings for superconducting windings[17].

2) Vanadium-Cobalt-Iron (Hyperco).

These alloys are produced in strip form containing a small Niobium (Nb) addition to gain refining during the processing of the final heat treatment plant of the strip. This type of treatment has been used mainly in the manufacture of rotor and stator lamination in motors and generators for power generation applications in aircraft, and more recently in electric vehicle magnetic bearings. The Hy50 alloy have a nominal composition of 0.01% C, 0.05% Mn, 0.05% Si, 0.05% Nb, 1.90% V and 48.75% Co-Fe.

III. IHyperco50 Alloy Electromagnetic and Thermal Characteristics.

In this chapter, the objective is to analyze the material Hyperco (Hy50), from the point of view of its electromagnetic and thermal characteristics on its potentiality when inserted in magnetic circuits of electric machines. For comparison, this alloy will be compared to the material Ferro Silicon (Fe-Si) which is a typical material in electric machines.

A. Electromagnetic Characteristics

Of the main electromagnetic characteristics, the ones standing out are the magnetic saturation and permeability of the materials and the losses in the material when exposed to a variable magnetic field.

The saturation and magnetic permeability of materials, usually known as the B-H curve, is one of the characteristics with the upmost importance in the design of electric machines. This indicates the level of magnetic flux that the material is able to withstand and which in turn is intrinsically linked to the source of the losses of magnetic origin in the material.

1) Electromagnetic Characteristics

For the determination of the B-H curve of the Hy50 alloy, a magnetic core formed of the following dimensions is constructed, consisting of two parts, one "E" shaped and one "I" shaped, Fig. 1. In the center column of the magnetic circuit are placed two copper windings, the primary and the secondary, each one with N turns. The magnetic flux density created by the coils can be measured directly through a Hall effect probe, Fig. 2, or indirectly through the induced voltage at the secondary winding.

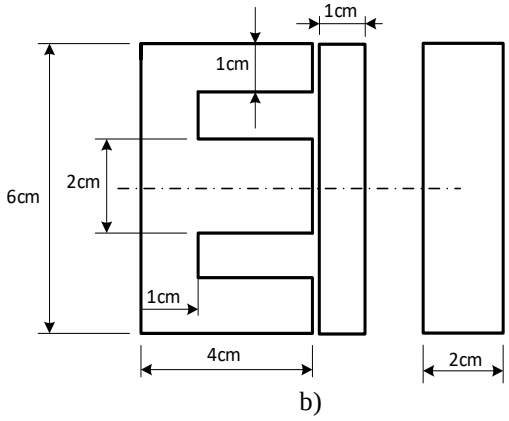

Fig. 1: Developed prototype dimensions of the core formed by "E" and "I"

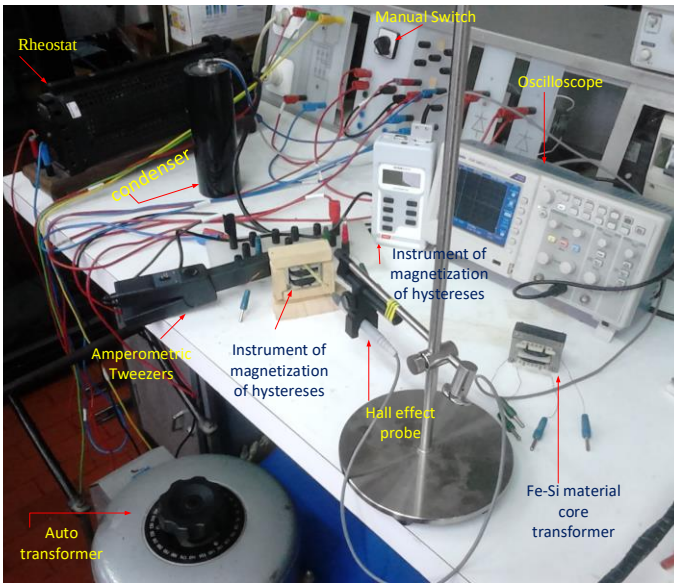

Fig. 2: Complete magnetic circuit assembly with Hall effect probe for measuring the magnetic field under test.

In parallel, the same circuit was also constructed in Fe-Si material, to carry out the same tests as in the Hy50 material. With this it is possible to obtain a basis of comparison between the new alloy and the classic materials used in machines.

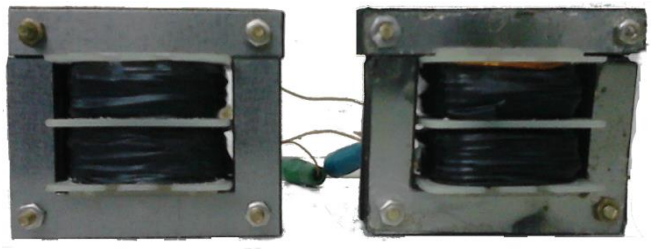

Fig. 3: Transformer developed for the realization of the tests: left made of Fe-Si and to the right of Hy50.

After measuring the current imposed on one of the windings, it is possible to estimate the intensity of the magnetic field, *H*. For the estimation of the intensity of the field *H*, the integral formulation of the law of Ampère given by equation (1) was used, relating the magnetic field to the current. Based on the dimensions of the magnetic circuit developed, Fig. 4, and through equation (1), it is possible to obtain the relation described by equation (2), where H_r, H_l and H_c represents the magnetic field strength in the right, left and center columns of the magnetic core, respectively.

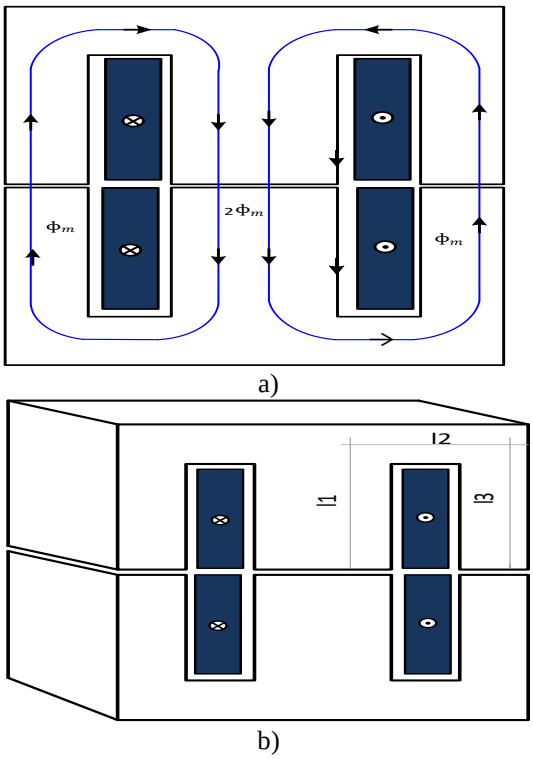

Fig. 4: a) - EE 2D magnetic circuit; b) - EE 3D magnetic circuit.

$$\oint_C \boldsymbol{H}\, d\boldsymbol{l} = \iint \boldsymbol{Jn} ds \qquad (1)$$

$$\oint_C \boldsymbol{H}\, d\boldsymbol{l} = NI \leftrightarrow$$

$$2H_c l_1 + 2H_{rd}(l_2 + l_3) = NI \qquad (2)$$

Assuming the homogeneity of the magnetic core and neglecting the magnetic leakage in the circuit, it is possible to relate the magnetic field values between each column, through the law of the cuts.

$$\sum_{\circlearrowleft} \phi_i = 0 \qquad (3)$$

$$\phi_{re} + \phi_{ld} = \phi_c \qquad (4)$$

By the symmetry of the circuit results $\phi_{re} = \phi_{ld}$ and as the sections of the lateral columns are double the central one gets:

$$\begin{cases} \phi_{re} = B_{re} S \\ \phi_c = B_c 2S \\ \phi_{ld} = B_{ld} S \end{cases} \rightarrow B_{re} = B_{ld} = B_c = B \qquad (5)$$

Thus, it can be considered that the magnetic field intensities in each column of the circuit have equal values. Then, the following relationship is described by equation (6).

$$2H(l1 + l2 + l3) = NI \leftrightarrow H = \frac{NI}{2(l1+l2+l3)} \qquad (6)$$

For the determination of the magnetic induction field, two methodologies were used: 1) the direct measurement of the field through the use of a Hall effect probe or 2) through the indirect measurement, applying the general law of induction, resulting from the voltage measurement. to the winding terminals.
For the indirect determination of the field of magnetic induction, the general law of induction was applied.

$$\oint \boldsymbol{E}\, d\boldsymbol{l} = -\frac{d\boldsymbol{\Psi_2}}{dt} \Leftrightarrow u_2 = \frac{d\Psi_2}{dt} \Leftrightarrow u_2 = \frac{d(NBS)}{dt} \Leftrightarrow$$

$$B = \int_0^t \frac{u_2}{NS} dt \qquad (7)$$

2) Methodology for Estimating Core Losses

The methods used here to determine the losses in the core were the following two indirect methods: 1) through the power balance in the circuit or 2) through the variation of magnetic energy during a cycle of variation of the magnetic field.

$$P_{cu} = RI_{ef}^2 \qquad (8)$$

$$P_{in} = U_{ef} I_{ef} \cos\varphi \qquad (9)$$

$$P_{fe} = P_{in} - P_{cu} \approx \frac{\boldsymbol{W_{diss\ hyst}}}{\boldsymbol{\Delta T}} \qquad (10)$$

3) Methodology for Obtaining the BH Curve of Materials.

In order to obtain the B-H characteristic of the new Hy50 alloy, experimental tests were carried out on the magnetic circuit shown in fig. 1, by applying voltage pulses to obtain higher values of currents Fig. 5.

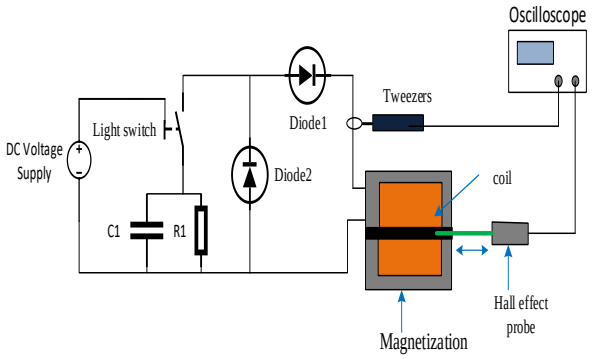

b)

Fig. 5: Circuit for application of voltage pulses.

Results for the voltage pulses in the magnetic pulse are shown in Table. 1. The values correspond to the maximum amplitude of the current, voltage and magnetic fields.

Table. 1: Impulse test result

Applied voltage	Fe-Si			Hy50		
U [V]	I [A]	B [T]	H [A/m]	I [A]	B [T]	H [A/m]
10	6	0,31	3060	7,6	0,12	3876
15	10	0,47	5100	12,7	0,20	6477
20	13	0,64	6630	17,4	0,28	8874
25	20	0,94	10200	21	0,29	10710
30	25	1,021	12750	22,5	0,37	11475
35	29	1,09	14790	30	0,44	15300
40	34	1,09	17340	32	0,46	16320
45	40	1,14	20400	39	0,49	19890
50	44	1,21	22440	44	0,54	22440
60	54	1,22	27540	52	0,58	26520
70	62	1,26	31620	60	0,67	30600
100	92	1,46	46920	91,2	0,74	46512
150	138	1,62	70380	122	0,89	62220

With the obtained results, we sought to understand why the magnetization curve obtained for the material Hy50 is lower than the Fe-Si one, when it is known this can reach 2T before the magnetic saturation, Fig. 6. It was concluded that this difference is due to the fact that the material did not had the necessary treatments for its finalization.

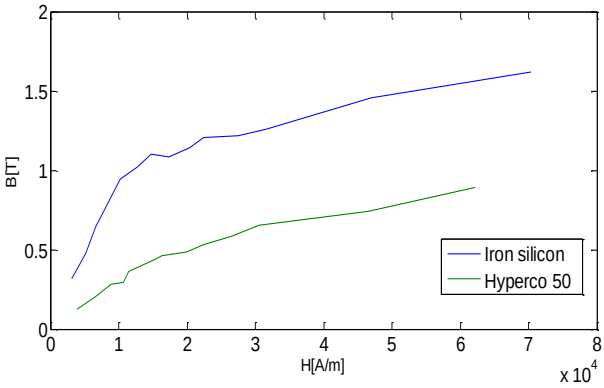

Fig. 6: Positive region BH curve of Fe-Si and Hy50

4) Experimental Tests for Determination of Magnetic Core Loss.

For the determination of losses in the magnetic core of Hy50 material experiments were performed on the developed magnetic circuits. For such, alternating sinusoidal voltages were applied to the circuit primary, keeping the secondary in an open circuit. For the first tests, the value of the losses in the core was determined through the power balance, (10) for several applied current and voltage values.
The results obtained are listed in Table. 2 and Table. 3 for the Fe-Si and Hy50 circuit, respectively.

Table. 2: Results of the Fe-Si AC assay.

In primary		Powers				Losses			
voltage	Current								
V_{ef} [V]	I_{ef} [V]	P [W]	Q [Var]	S [VA]	cos(φ)	P_{cu} [W]	P_{ef} [W]	P_{ef} [W/kg]	Pt [W]
12,2	6,29	40,7	62,9	74,6	0,54	27,7	13,0	40,9	40,7
7,3	3,52	10,6	23,4	25,7	0,42	8,7	1,9	6,1	10,6
5,9	2,78	6,9	15	16,6	0,42	5,4	1,5	4,7	6,9
5,1	2,34	5	10,8	11.9	0,42	3,8	1,2	3,7	5
4,4	2,1	3,8	8,3	9,1	0,42	3,1	0,7	2,2	3,8
3,6	1,7	2,7	5,4	6	0,45	2,0	0,7	2,1	2,7
2,9	1,35	1,8	3,5	3,9	-	1,3	0,5	1,6	1,8
2,1	0,97	0,8	1,8	2	-	0,7	0,1	0,4	0,8
0,3	0,15	0	0	0	-	0,0	0,0	0,0	0

Table. 3: Hy50 AC assay results.

In primary		Powers				Losses			
voltage	Current								
V_{ef} [V]	I_{ef} [V]	P [W]	Q [Var]	S [VA]	cos(φ)	P_{cu} [W]	P_{fe} [W]	P_{fe} [W/kg]	PT [W]
7,1	6,4	42,9	13,1	44,5	0,96	28,7	14,2	44,7	42,9
5,8	5,03	27,9	8,3	29	0,96	17,7	10,2	32,0	27,9
5,1	4,81	23,4	7,6	24,6	0,95	16,2	7,2	22,7	23,4
4,5	4,45	18,7	6,5	19,8	0,94	13,9	4,8	15,2	18,7
3,7	3,79	13	4,7	13,9	0,94	10,1	2,9	9,3	13
2,8	3,01	7,8	2,9	8,3	0,94	6,3	1,5	4,6	7,8
2,4	2,65	5,9	2,2	6,3	0,92	4,9	1,0	3,1	5,9
0,1	0,16	0	0	0	-	0,0	0,0	-0,1	0

From the experimental results, the first aspect to be noted is that the materials have similar core loss values for similar magnetic field values, i.e., similar current values. As an example, it can be seen that for a current close to 6.3A, the losses in the core are about 44.7W / kg for the alloy of Hy50 and 40.9W / kg for Fe-Si, Fig 7.

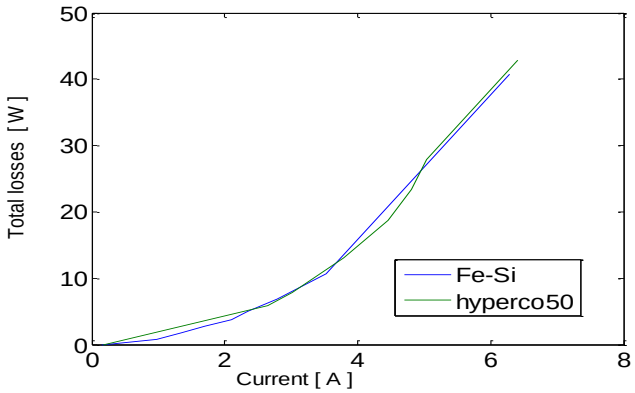

Fig 7: Evolution of iron losses as a function of Fe-Si and Hy50 current.

Based on the experimental results, we obtained B-H curve Fig. 9, where we compare the experimental values obtained with the ones from the datasheet of the material.

.

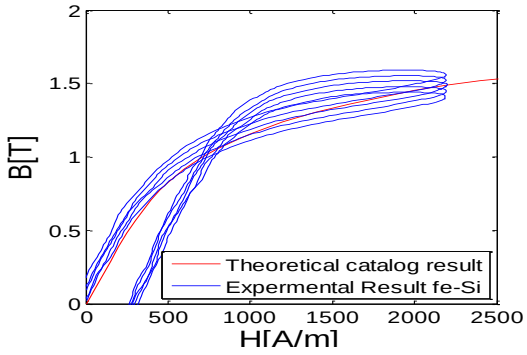

Fig. 9: Hysteresis curve: Experimental comparison with result of the datasheet.

To confirm the results obtained through the power balance a second test was performed measuring the flow value in the core and calculating the respective values of losses in the core through the B-H curve. In order to perform this test, a second larger E-I circuit of Fe-Si was used, Fig. 8.

Fig. 8: Transformer of the Fe-Si core.

Through the obtained results, it is possible to calculate the area of the lost magnetic energy in each cycle and through it, calculate the losses in the core of Fe-Si. Using an approximation of the area of magnetic energy lost per cycle, Fig. 10.

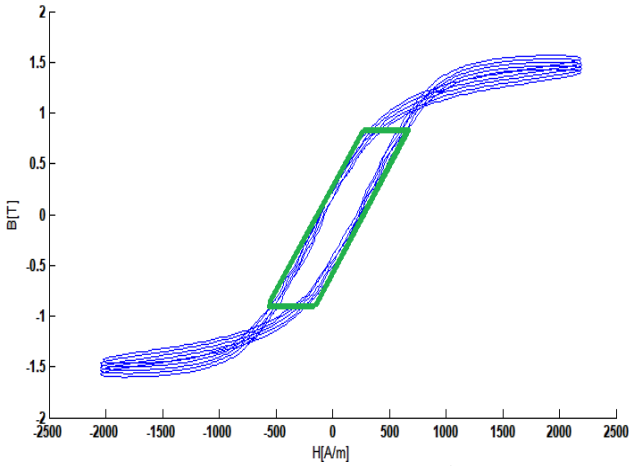

Fig. 10: Curva de Hysteresis por obtensao do fluxo e corrente

Table. 4 shows the experimental values obtained for Fe-Si. With these results it was possible to compare with the catalog results, in order to verify the magnetic properties. In Table. 5, it is possible to verify that the values correspond to those of the alloy used in the circuit, M400-50A.

Table. 4: Experimental results of assay in AC regime.

d [kg/m^3]	V [m^3]	P [kg]	Pfe [W]	Pcu [W]	Pfe [W/ kg]	PT [W]
7,6x10^{+3}	7.13 x10^{-4}	5.42	18	4.4	3.7	19.8

Table. 5: Catalog Results.

Designation Standard	s	ρ	Maximum core loss AT		
	[mm]	[kg/m^3]	50Hz; 1.5T W/kg	50Hz; 1.0T W/kg	60Hz; 1.5T W/lb
M270-35A	0.35	7.65	2.70	1.10	1.55
M300-35A	0.35	7.65	3.00	1.20	1.72
M400-50A	0.50	7.70	4	1.7	2.3
M470-50A	0.50	7.70	4.70	2	2.70
M530-50A	0.50	7.70	5.30	2.30	3.05

5) *Comparison of Magnetic Properties Among Materials*

Table 3 shows the results of the comparison of the two circuits in terms of weight, density, volume and losses. If we compare to the same magnetic field value, for example, with a current of 6.3A (Table. 2 and Table. 3), it is verified that the losses in the core have similar values.

Table. 6: Results between o FS e HY

	P [kg]	ρ [kg/m^3]	V [m^3]	Pfe [W]	Pcu [W]	Pfe [W/ kg]	PT [W]
Fe-Si	0.3	7.6x10^3	4.12x10^{-5}	1	39	3	40
Hy50	0.3	8.11x10^3	3.86x10^{-5}	0.6	32	2	33

In order to verify the level of the losses in the core for different values of field B. a simulation in finite elements with the curves B-H of the different materials was used, with curves B-H of Fig.11.

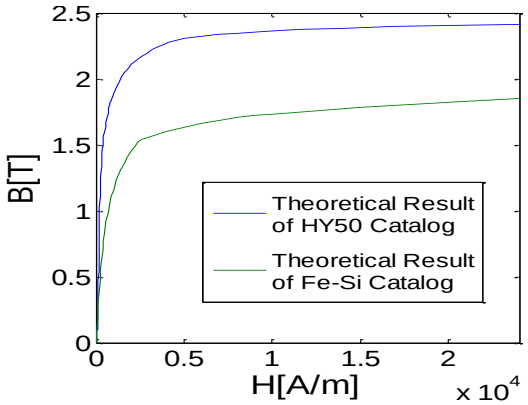

Fig.11: B-H curves used in the simulation of materials.

B. *Thermal Model in Concentrated Parameters.*

The construction of a thermal model in Lumped Parameter Thermal Model (LPTM) allows the estimation of the temperature of the developed system without using finite element tools. The equation that governs the propagation of the heat in steady state is described in *(12)*, where T_{sup} and T_{amb} are the surface and ambient temperatures, P_J represents the losses by heat dissipation in the copper and iron materials and R_{conv} corresponds to the thermal resistance of convection of the heat. The convection thermal resistance is defined in (2) where *h* is the convection coefficient and corresponds to the lateral surface of the cylinder.

Equation *(11)* shows the calculation of the thermal convective resistance, where r_{int} and r_{ext} are the inner and outer radii of the cylinder base and K_{th} corresponds to the thermal conductivity of the metal.

$$R_{cond;cu;fe} = \frac{l}{2\pi K_{th} l} ln\left(\frac{r_{ext}}{r_{int}}\right) \quad (11)$$

$$T_{sup} = R_{conv} P_J + T_{amb} \quad (12)$$

$$R_{conv} = \frac{1}{hSup} \quad (13)$$

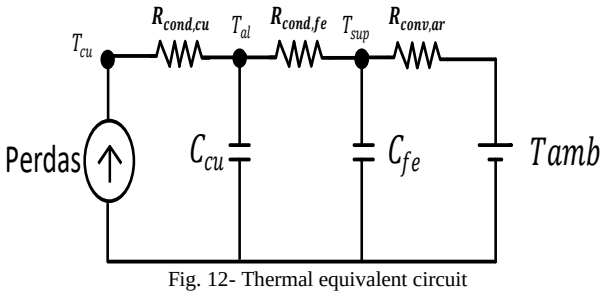

Fig. 12- Thermal equivalent circuit

Based on the equations (12) and (14), the values of the thermal resistance of convection and conduction of copper and iron materials were determined Table. 7. The values of temperature reached by magnetic circuits at the different saturation points of Fe-Si and Hy50 materials are presented in Table. 8.

Table. 7: Result of driving resistance

-	Lightning [cm]	Driving Resistance	
outdoor	3.1	copper	0.000233
interior	2.1	iron	0.000339
-	Convection coefficient h [W/m^2K]	Air Convection Resistance	
Hyperco	7.51	2.22	
Iron Silicon	5.49	3.04	

Table. 8: Thermal output of the MTPC

	R [m]	D=2R [m]	S [m^2]	P_{fe}[W] @ 50 [HZ]	Pcu [W]	T_{amb} [°C]	T_{sup} [°C]
Hy50	0.02	0.05	0.1	52.5	4	20	117
Fe-Si				18.03	4		48

The following figure shows the evolution of the temperature at the surface of the circuit during the experimental test. As it can be seen, the temperature begins to stabilize at about 44 ° C after 1 hour and 20 minutes. This value is in agreement with the values obtained through the LPTM for the Fe-Si.

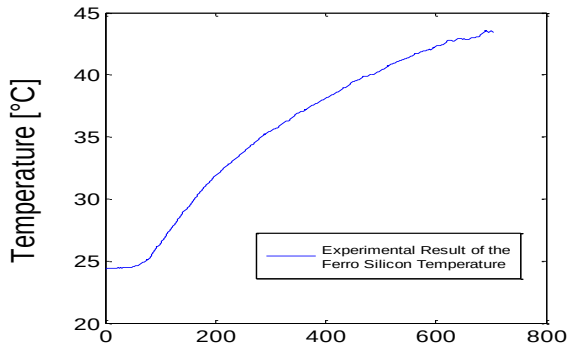

Fig. 13- Experimentally obtained iron silicon temperature

C. *Finite Element Simulation*

In order to develop a more detailed model of the magnetic circuit it is possible to obtain more detailed results of the temperature profile with a finite element model of the magnetic circuit.

According to the numerical results, it is verified that the temperature level of both the magnetic circuit and the material Hy50 and Fe-Si meet the expected values through the LPTM and the experimental results, Fig. 14.

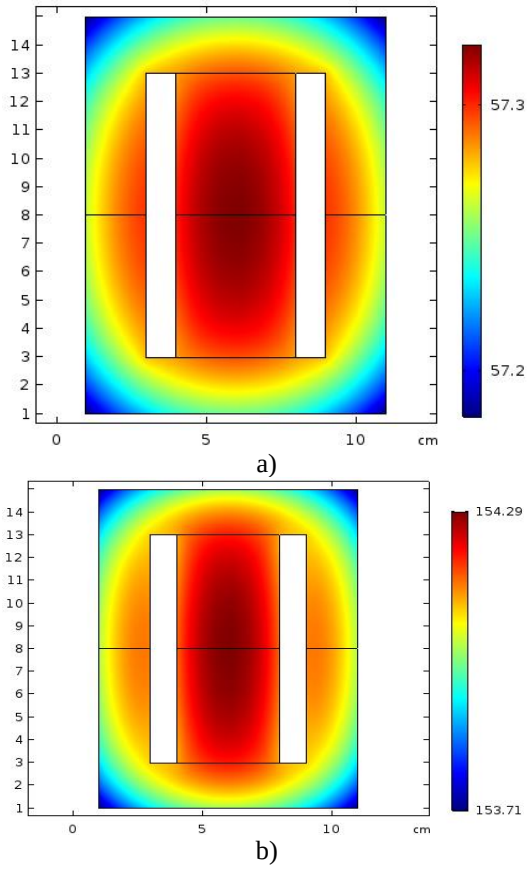

Fig. 14. Temperature in a) Iron Silicon and b) Hyperco.

In Table. 9, the results are more or even in the same order of magnitude. It can be concluded that these results are in the same range of the ones obtained experimentally.

Table. 9: Comparison of thermal simulation results

	Experimental	Model MTPC	Finite elements
	[°C]		
Hy50	-	117.0	154.3
Fe-Si	47.7	47.7	57.3

IV. Pre-Sizing a Hy50 Alloy Transformer

The work carried out in this chapter is aimed at the pre-sizing of single-phase transformers with the different Fe-Si and Hy50 alloys. The purpose of this work is to compare the electrical and thermal performance of the transformers of each material alloy.

A. *Single Phase Transformer Equivalent Electrical Circuit*

For the study of the electrical behavior of the single-phase transformer, a system of equations was developed, based on concentrated parameters. This system of equations was developed based on the general induction and Ampère laws,

applied to the primary and secondary windings of the transformer, by equation (14). u_1, u_2, i_1 e i_2 are the voltages and currents of the primary and secondary transformer, R_1 and R_2 are the resistors of the respective windings and $\Psi_1$and Ψ_2 each linkage flux.

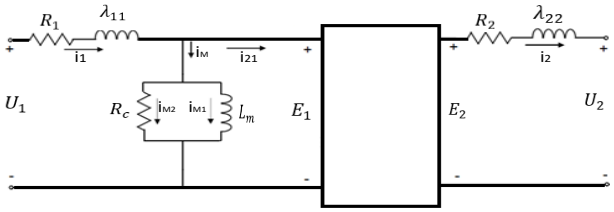

Fig. 15. Transformer equivalent circuit

$$\begin{cases} u_1(t) = R_1 i_1(t) + \dfrac{d\Psi_1(t)}{dt} \\ -u_2(t) = R_2 i_2(t) + \dfrac{d\Psi_2(t)}{dt} \end{cases} \qquad (14)$$

The total linkage flux with the primary and secondary can be calculated by separating the primary and leakage flux, equation (15).

$$\begin{cases} \Psi_1(t) = \Psi_{1p}(t) + \Psi_{1\lambda}(t) = N\phi_N(t) + \Psi_{1\lambda}(t) \\ \Psi_2(t) = \Psi_{2p}(t) + \Psi_{2\lambda}(t) = N\phi_N(t) + \Psi_{2\lambda}(t) \end{cases} \qquad (15)$$

The determination of the coefficients is done using the results of finite element simulation of the circuit in 3D.

$$\begin{cases} L_{11} = \left.\dfrac{d\Psi_1}{di_1}\right|_{i_2=0}, L_{22} = \left.\dfrac{d\Psi_2}{di_2}\right|_{i_1=0} \\ L_M = \left.\dfrac{d\Psi_1}{di_2}\right|_{i_1=0} = \left.\dfrac{d\Psi_2}{di_1}\right|_{i_2=0} \\ \lambda_{11} = L_{11} - L_M \\ \lambda_{22} = L_{22} - L_M \end{cases} \qquad (16)$$

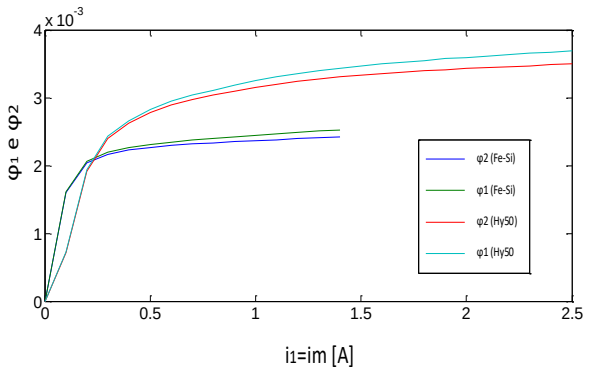

Fig. 16 : Magnetic flux between coil 1 and 2 for Fe-Si and Hy50.

Based on the results presented in Fig. 16, we obtain the evolution of the mutual induction and dispersion coefficients with the magnetization current through equations (17).

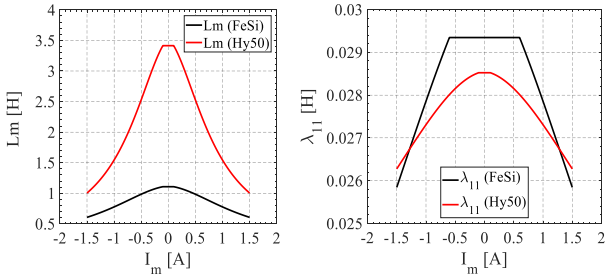

Fig. 17 : Coefficient of mutual and dispersion of the circuit in Fe-Si and Hy50.

B. *Simulink Model Development*

The system of equations representing the single-phase transformer (equations (14) to (17), together with the evolution of the induction coefficients with the magnetization current, is a non-linear system. For the calculation of the solution of the system, the numerical tool Simulink was used. Based on the equations described above and knowing that the voltage in the primary of the transformer and its secondary load will be imposed, a block model was developed.

$$\begin{cases} u_1 = R_1 i_1 + \dfrac{d\Psi_1}{dt} \\ -u_2 = R_2 i_2 + \dfrac{d\Psi_2}{dt} \end{cases} \Rightarrow \begin{cases} \Psi_1 = \int (u_1 - R_1 i_1)\, dt \\ \Psi_2 = \int (-u_2 - R_2 i_2)\, dt \end{cases} \qquad (17)$$

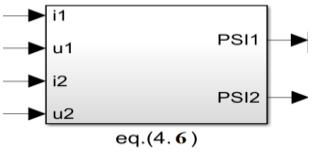

Fig. 18 : block containing the equations in (17).

The following figure shows the overall model of the single-phase transformer circuit, Fig. 19. This circuit already considers the saturation curve of the materials but does not yet consider the losses in the iron.

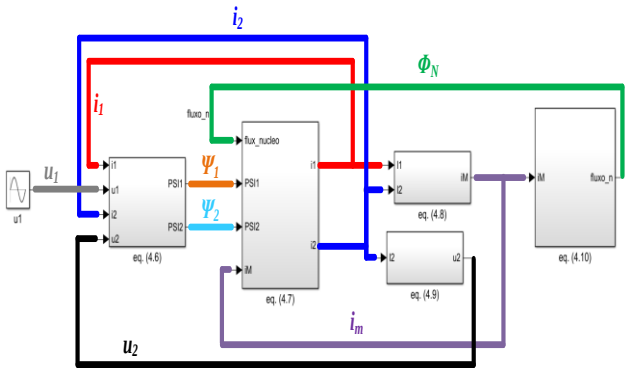

Fig. 19 : Lossless single-phase transformer model.

The losses in the iron can be calculated from the magnetization voltage and through the equation. (18). In this way the resistance representing the losses in the iron can be calculated by the equation. (19).

$$P_{fe} = \frac{U_{m\,ef}{}^2}{R_{fe}} \leftrightarrow \quad R_{fe} = \frac{U_{m\,ef}{}^2}{P_{fe}} = \frac{U_{m\,ef}{}^2}{K\phi_N{}^2} \qquad (18)$$

Thus, three new equations arise with the resistive component of the magnetization current, im2, the determination of the magnetization voltage, one, and the reactive component of the magnetization current, i_{m1}.

$$u_m = \frac{d\phi_N}{dt} \qquad (19)$$

$$i_{m2} = \frac{u_m}{R_{fe}} \qquad (20)$$

$$i_{\mathrm{m1}} = i_{m-}i_{m2} \qquad (21)$$

The new transformer model schematic is shown in Fig. 20. Only the new blocks of equations (19) to (21) and the connections marked in dashes have been added.

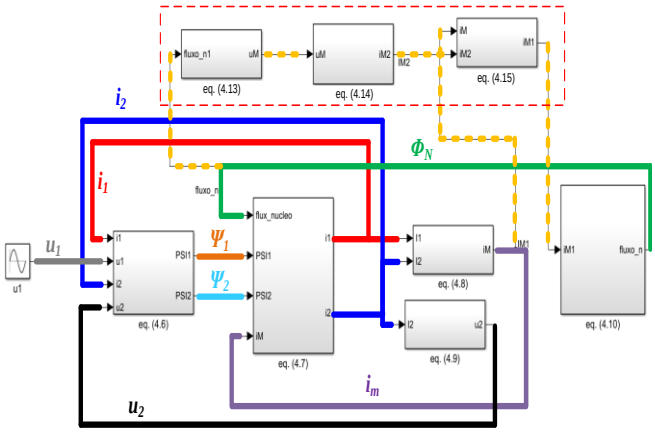

Fig. 20 : Model of single-phase transformer with losses.

C. Simulation Results

Based on the model developed and implemented in Simulink, the results of the transformer operating point were obtained with the Hy50 and Fe-Si materials.

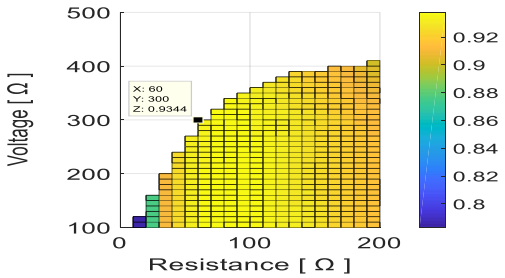

a)

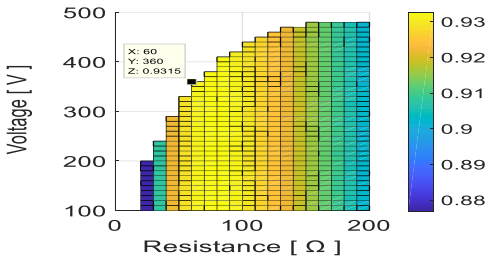

b)

Fig. 21: Efficiency for a) Fe Si and b) Hy50

Results show that, if the operation point is limited to the same temperature of 120ºC, the Fe-Si presents the highest output power, with higher results than the Hy50. However, if considering operation point in the best BH point for each material, the Hy50 presents almost more than 50% of output of the Fe-Si, but with a higher temperature. This means that it is possible to obtain more specific power with Hy50 however it is important to consider its required auxiliary cooling system.

Table. 10: Comparison results, limited in temperature and knee saturation point, between Fe-Si and Hy50.

	Results - limiting copper temperature to 120 ° C		Results - limiting to saturation point BH (Hyperco-2T and FeSi-1.4T)		units
	FeSi	Hy50	FeSi	Hy50	
Us	300	320	300	410	V
RL	60	80	60	80	Ω
η	93,4%	93,2%	93,4%	93,2%	%
P1	643,6	610,9	643,6	1001	W
Pfe	15,34	23,31	15,34	38,16	W
Pcu	26,87	18,19	26,87	29,87	W
P2	601,3	569,4	601,3	933,3	W
i1ef	3,49	2,823	3,49	3,62	A
i2ef	3,195	2,681	3,195	3,433	A
u1ef	212,1	226,3	212,1	289,9	V
u2ef	191,7	214,5	191,7	274,6	V
Bef	0,98	1,08	0,98	1,383	T
Bpico	1,38	1,53	1,38	1,96	T
Lmeq	0,906	3,2	0,906	3,032	H
Tcu	119,2	117,5	119,2	179,8	°C

V. Conclusions and Future Work

This study was based on laboratory tests, which allow the characterization of the Vanadium-Cobalt-Iron (Hyperco) alloy, namely in the measurement of the BH curve and losses by hysteresis. With the alternating voltage tests, it was not possible to obtain magnetic induction fields close to the saturation values of the materials, therefore testing was done with current pulses. The losses in the iron were calculated through two methodologies: 1) through the power balance in the transformer and 2) through the inner area to the hysteresis curve, which corresponds to the energy dissipated by hysteresis cycle. To, obtain a better finish the material should have been

boiled at 865 ° C for 4 hours in dry hydrogen and followed by cooling at a rate of 85 ° C / h to room temperature. However, the first, in order to achieve the required properties, in particular its high saturation point, it is important to analyze the possible forms of additional cooling required to compensate the hysteresis. From the simulation of a transformer with Fe-Si and Hy50, it was concluded that the Hy50 allows an increase of about 50% of specific power, however, will require an additional cooling system.

REFERENCES

[1]. ASTM A697/A697M, "Standard test method for alternating current magnetic properties of laminated core specimens using Voltmeter-ammeter-Wattmeter method", *ASTM* (2004), Available at: http://compass.astm.org/Standards/HYSTORICAL/A697A697M-03.htm.

[2]. Cartech.com. "Carpenter - CarTech® Hiperco® 50 Alloy". [online] Disponível em: https://www.cartech.com/en/product-solutions/cartech-hiperco-50-alloy/ [Acedido a 2 Out. 2018].

[3]. R.M. Bozorth, Ferromagnetism, "IronSilicon Alloys", *NeW York: IEEE Press*, vol 32,n.1, pp. 190–209. 1978.

[4]. C.W. Chen, " Metallurgy and magnetic properties of an Fe-Co-V alloy", *Journal of Applied Physics*, vol. 69 n.3, pp.348, 1961.

[5]. Q. Zhu, " An increase of structural order parameter in Fe–Co–V soft magnetic alloy after thermal aging ", *Applied Physics Letter*, vol. 69, 3917, 1998.

[6]. D.W. Clegg and R.A. Buckley, "Order Transformation in Iron–Cobalt-Based Alloys", *Metal Science Journal*, vol 7, pp. 48-54 , 2018.

[7]. A.W. Smith and R.D. RaWlings, Phys, "The homogeneity range and defect structure of the laves phase $NbFe_2$", *Status Solidi A*, vol 34, pp117 ,1976.

[8]. M. RajkoVic and R.A. Buckley, "Ordering transformations in Fe-50Co based alloys", *Metal Science Journal*, vol.15, pp21 ,1981.

[9]. A.I.C. Persiano and R.D. RaWlings, "physica status solidi " *Status Solidi A*, vol. 103, pp.574, 1987.

[10]. Q. Zhu, L. Li, M.S. Masteller, and G.J. Del Corso, " Microstructure and Hall–Petch Behavior of Fe–Co-based Hiperco© Alloysa)", *Applied Physics Letter*, vol.69, pp.25,1996.

[11]. L. Li, J. . "Applications of Ferromagnetic and Optical Materials, Storage and Magnetoelectronics:", *Journal of Applied Physics*, vol.79, pp.4578 ,1996.

[12]. D. SHyn, J. Degauque, C. Lebourg, and B. Astie, "Influence of Thermal Treatment on Magnetomechanical Damping of 49Fe-49Co-2V Alloy", *Journal De Physique IV Colloque*, vol.06, pp. C8-545,1996.

[13]. Z. Turgut, M.Q. Huang, K. Gallagher, M.E. McHenry, and S.A. Majetich, J. Appl, "Magnetic properties and ordering in C-coated FexCo1−xFexCo1−x alloy nanocrystals", *Phys*. Vol 81, pp.8, 1997.

[14]. Y. Ustinovs HykoV,B.Pushkare V, I. Shabanova, and A.Ulinova, " Phase Transformations in the Fe-Co System ", *Interface Sci*., vol.10, pp.311 ,2002.

[15]. X.M. Cheng, X.K. Zhang, D.Z. Zhang, S.H. Lee, A. Duckham, T.P. Weihs, R.C. Cammarata, J.Q. Xiao, and C.L. Chein, J, "Preparation and characterization of MnZn-ferrite nanoparticles using reverse micelles", Appled Physics, Vol.93, pp.7121 (2003).

[16]. B.D. Cullity and C.D. Graham, "Introduction to Magnetic Materials", Wiley IEEE Press, n.2, pp. 466, 2009.

[17]. P. Tixador, F. Simon, H. Daffix, M. Deleglise, "150-kW Experimental Superconducting Permanent-Magnet Motor", IEEE. Trans. Applied Superconductivity., vol.9, n.2, Pp. 1205-1208, Junho 1999.